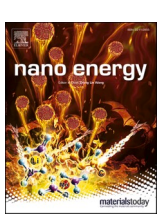
ELSEVIER

Contents lists available at ScienceDirect

Nano Energy

journal homepage: www.elsevier.com/locate/nanoen





Optimizing molecular light absorption in the strong coupling regime for solar energy harvesting

Steven Chavez, Suljo Linic

Department of Chemical Engineering, University of Michigan - Ann Arbor, 2800 Plymouth Road, Ann Arbor, MI 48109, USA

ARTICLE INFO

Keywords: Strong coupling Solar energy harvesting Cavity quantum electrodynamics Polaritons

ABSTRACT

The strong coupling of optical absorbers (e.g., molecules or semiconductors) to confined photonic modes fundamentally alters the physical properties of the coupled system via the formation of hybrid light-matter states. One potential application of strong light-matter coupling relies on exploiting it to localize light-induced charge excitation processes to small volumes of material. Applications that would benefit from this localization include thin-film photovoltaics, photodetection, photocatalysis, and others, where the overall performance depends on the ability of a material to amplify light absorption (i.e., the formation of electron-hole pairs) within specific locations in space. This contribution investigates how strong light-matter coupling affects light absorption rates in molecular absorbers coupled to photonic nanostructures. Our results show that the molecular light absorption efficiencies are highest in configurations where the strongly coupled molecules interact directly with the incoming photon flux. We also identify a nonlinear dependence in the molecular absorption as a function of concentration, unique to the strongly coupled systems. Based on these results, we propose design principles for engineering nanostructured systems that allow for high efficiencies of charge carrier localization into strongly coupled absorbers.

1. Introduction

Interactions between light and matter can significantly change when confined inside a photonic structure [1–6]. For example, electronic transitions in an absorber (emitter) such as a dye molecule can hybridize with a confined electromagnetic field. This light-matter hybridization is a quantum phenomenon similar to the hybridization of electronic states when atoms form chemical bonds [7]. This hybridization can be achieved experimentally by placing the emitter within the vicinity (or inside) of a photonic or plasmonic structure that supports high-intensity electric fields. A typical example is a Fabry-Perot optical cavity consisting of two parallel metallic mirrors [6,8]. In this case, a simple dipole interaction governs the interaction strength (V) between an emitter and the cavity:

$$V = \overrightarrow{d} \bullet \overrightarrow{E} \tag{1}$$

where, \overrightarrow{d} is the transition dipole moment of the emitter in the cavity, and \overrightarrow{E} is an operator representing the electric field of electromagnetic radiation confined by the cavity[9] Physically, V is proportional to the

rate of energy exchange between the emitter and the cavity.

The extent of the light-matter hybridization depends on the magnitude of V relative to the rate of the energy dissipation pathways in the system (Scheme 1). These dissipation pathways include the decay rate of the emitter excited state (represented by the decay constant Γ_e) and the decay rate of the photon in the cavity (represented by the decay constant Γ_c). In the limit of slow cavity-emitter energy exchange compared to the energy dissipation rates, i.e., when $V < < (\Gamma_e, \Gamma_c)$, the system is in the weak coupling regime (Scheme 1a). When weakly coupled, the individual energy levels of the emitter and the cavity remain distinct. However, we can still observe some modifications of the emitter's physical behavior. A common example is the enhanced fluorescence of an emitter placed in an optical cavity due to the alteration of the emitter emission channels – known as the Purcell effect [10]. When the rate of energy exchange becomes faster than any available energy dissipation pathway in the system, i.e., when $V > (\Gamma_e, \Gamma_c)$, the system enters the strong coupling regime (Scheme1b). The strong emitter-cavity coupling results in the emergence of two hybrid light-matter energy states known as polaritons, resulting from the splitting of the emitter energy levels. The upper (P +) and lower (P-) polaritons are separated equally from the initial energy of

E-mail address: linic@umich.edu (S. Linic).

^{*} Corresponding author.

the emitter electronic transition (when the cavity resonance and emitter energy perfectly overlap). The total splitting is given by the Rabi splitting energy ($\hbar\Omega_R$). In the absence of dissipation, the expression for $\hbar\Omega_R$ is given by:[6].

$$\hbar\Omega_R = 2V_N = 2 \quad \overrightarrow{d} \bullet \overrightarrow{E} = 2d\sqrt{\frac{\hbar\omega}{2\varepsilon_0\nu}} \times \sqrt{n_{ph} + 1}$$
(2)

where V_N is the collective interaction strength for N molecules in the cavity, ε_0 is the vacuum permittivity, ν is the volume of the confined electromagnetic mode, $\hbar\omega$ is the resonant energy, and n_{ph} is the number of photons in the cavity.

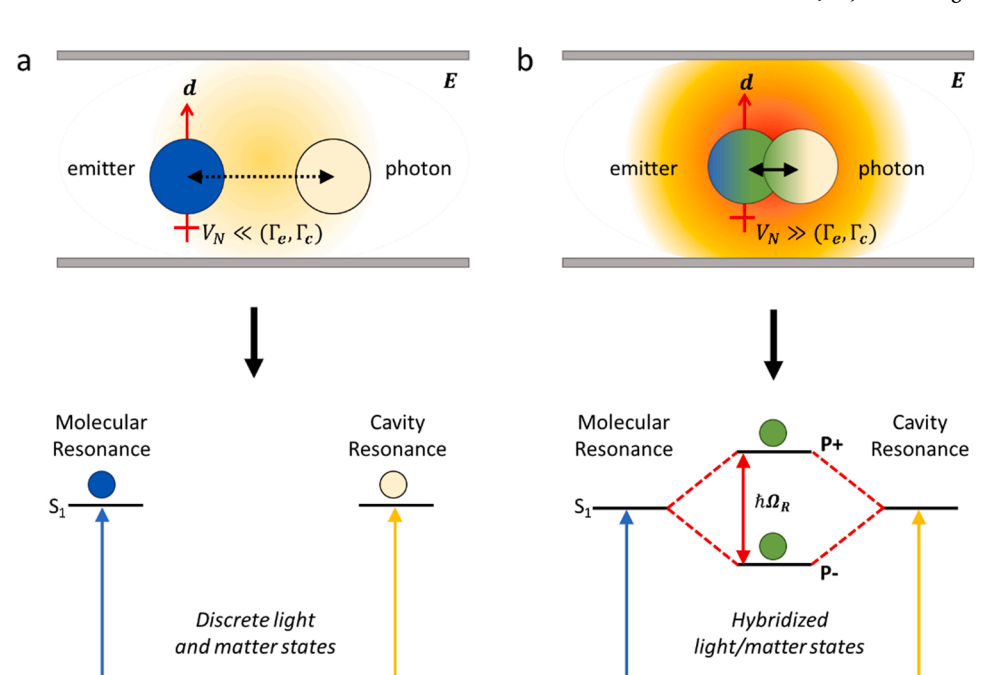
Eq. (2) indicates several mechanisms to increase the value of $\hbar\Omega_R$ and thus the probability that the system will enter the strong coupling regime. These include ensuring that the electromagnetic mode of the cavity is resonant with the emitter electronic transition (allowing them to exchange photons of the same energy), designing cavities with high electric fields compared to the free space electric field, which can be accomplished by confining the electric field into small volumes (i.e., decreasing ν), and increasing the magnitude of dipole moment (d) of the emitter coupled to the cavity. For N emitters in the cavity, d is a collective dipole moment and can be increased by increasing the concentration of molecules in the cavity. Experimentally, the transition from the weak to strong coupling regime can be probed by monitoring the splitting in the cavity absorption peak (i.e., the emergence of P + and P-) via optical spectroscopy.

The emergence of polaritons in strongly coupled systems implies that the system's physical properties are fundamentally altered [4–6,9,11,12]. For example, it has been demonstrated that strong coupling induces modifications of the work function of dye molecule films [13], increases the rate/distance of nonradiative energy transfer between donor and acceptor molecules [14–18], enhances electron transfer in metal-semiconductor systems [19,20], increases the charge conductivity of organic semiconductors [21–23], and changes the rate/selectivity of chemical reactions by coupling of electronic/vibrational modes of the reacting molecules to a cavity [24–30]. Another potential application of strong light-matter coupling relies on exploiting it to localize light-induced charge excitation processes to small volumes of material strongly coupled to a cavity. Practical applications that would benefit

from these processes include thin-film photovoltaics, photodetection, photocatalysis, and other applications where the overall performance often depends on the ability of a material to localize and amplify light absorption (i.e., the formation of electron-hole pairs) to small volumes $[31\mbox{-}38].$ In this context, localizing light absorption into thin layers of absorbing material is essential for increasing overall power conversion efficiency in these applications.

The question we seek to answer is whether one can exploit lightmatter coupling to confine solar energy into small volumes of optically active materials. We point out that a few reports have shown that strong coupling can enhance the overall light absorption in various systems. Typical examples include multicomponent systems that couple absorbing materials to metallic structures or single nanostructures that act as both the cavity and the absorbing material [39-41]. In these previous studies, it is generally unclear how the absorption process is spatially distributed throughout the system. For example, in Fabry-Perot optical cavities that contain two metallic mirrors, one would expect a significant fraction of absorption to occur directly in the mirrors and not in the absorbing material coupled to the cavity. Due to the short lifetime of charge carriers in metals, this absorption would lead to parasitic heating losses in the mirrors [42]. In this work, we quantify the impact of strong coupling on the localization of the absorption process in dve molecules coupled to a cavity. Localizing the light absorption to the dye molecules is critical for hot electron (hole) technologies because of the long lifetimes of charge carriers generated in molecules compared to metals. These longer lifetimes allow the potential extraction of these charge carriers to perform functions such as driving photo-catalytic reactions or serving as a driving force to enhance the electrochemical potential of charge carriers.

We use a combination of experimental and modeling approaches to investigate how the local light absorption rates (i.e., charge carrier generation) are modified within strongly coupled molecular absorbers. Our model system consists of 5,6-dichloro-2-[[5,6-dichloro-1-ethyl-3-(4-sulphobutyl)-benzimidazol-2-ylidene]-propenyl]—1-ethyl-3-(4-sulphobutyl)-enzimidazolium hydroxide, sodium salt, inner salt (TDBC) J-aggregate molecules coupled to a Fabry-Perot optical cavity consisting of two parallel silver (Ag) mirrors. We tune the system in and out of the strong coupling regime by varying the concentration of TDBC inside the cavities (i.e., increasing/decreasing *d*). We use this model system to



Scheme 1. Schematic and molecular state diagrams of an emitter with a transition dipole moment, \overrightarrow{d} , interacting with a photon confined in a metallic Fabry-Perot optical cavity (i.e., between two metallic mirrors). In the weak coupling regime (a), the interaction energy (V_N) between N emitters and the photon in the cavity is low. As a result, the emitter electronic transition and cavity resonance retain their individual character. If V_N becomes sufficiently high, the system enters the strong coupling regime (b), and two hybrid light-matter states (P + and P-) separated by the Rabi splitting energy $h\Omega_R$ emerge. Here, S_0 and S_1 represent the ground and the excited state of the emitter and \overrightarrow{E} corresponds to the magnitude of the electric field confined by the optical cavity.

analyze the critical parameters that govern the rate of charge excitation in the coupled system. Our results show that strong coupling offers opportunities to significantly amplify the absorption rates in the molecules coupled to the cavity. We demonstrate that effectively designed systems require significantly lower volumes and molecular concentrations to induce identical absorption rates as stand-alone molecular systems or the same system adsorbed on metallic mirrors. Based on these studies, we propose design principles for engineering nanostructured systems that allow for high efficiencies of charge carrier localization into strongly coupled absorbers.

2. Results and discussion

We fabricated three Fabry-Perot cavity systems for this study: one containing a high concentration of TDBC, one containing a low concentration of TDBC, and one containing no TDBC (See Fig. S1 for schematics of the fabricated systems). These cavities were fabricated to ensure their optical mode was resonant (tuned) to the TDBC electronic transition at 590 nm (See Fig. 1a). The cavities were fabricated by first depositing a 200 nm Ag film onto a piranha cleaned glass slide via electron beam evaporation at a rate of 5 A/s. Next, we prepared TDBCpolymer solutions of varying TDBC concentrations by dissolving either 1 wt% (low concentration) or 33 wt% (high concentration) of TDBC into aqueous solutions of polyvinyl alcohol (PVA). Here, wt% is the mass of TDBC divided by the total mass of TDBC and PVA in the solution. These solutions were filtered through a 0.22 μm nylon mesh and spin-cast onto the glass-supported Ag film to create PVA thin films loaded with the TDBC dye molecules. We determined the TDBC-PVA film thicknesses to be \sim 337 nm (PVA only), \sim 332 nm (low concentration), and \sim 203 nm (high concentration) using a combination of ellipsometry and profilometry measurements. We completed the cavities by evaporating a second, semi-transparent 30 nm Ag layer on top of the TDBC-PVA film.

We characterized the optical characteristics of the fabricated systems by analyzing their wavelength-dependent fractional absorption spectra using an optical integrating sphere. The fractional absorption (A) spectra for the cavity and mirror were obtained by measuring the samples' fractional reflection (R) at normal incidence and utilizing the equation A=1-R-T. We compared these absorption spectra to the absorption spectra of a few control samples (see Fig. S1): 1) *mirror systems* with the low and high concentration TDBC-PVA films coated onto 200 nm Ag films (with no top mirror), and 2) *stand-alone TDBC-PVA*

films of the low and high concentrations coated directly onto glass slides (with no top mirror). We chose metallic mirrors as a comparison instead of highly reflecting dielectric mirrors (i.e., Bragg reflectors) since dielectric mirrors typically exhibit high reflection in the IR, and our goal is to harvest visible light [43]. The thicknesses and concentrations of the TDBC-PVA layers in these control systems were identical to the thicknesses and concentrations of the TDBC layers in the cavity systems.

The data in Fig. 1a show that the pure PVA-Ag cavity supports two optical modes: one at $\sim\!400$ nm and one at $\sim\!590$ nm. The latter directly overlaps with the TDBC electronic transition. In the case of the low TDBC concentration (Fig. 1b), the cavity mode overlapping with the TDBC transition remains unperturbed (i.e., there is a single absorption band at 590 nm). This retention of the single cavity mode indicates that the concentration of TDBC in the cavity is not high enough to push the sample into the strong coupling regime. On the other hand, the data for the high concentration cavity (Fig. 1c) show an apparent splitting of the cavity mode due to the coupling of the cavity and TDBC electronic excitations. The absorption Rabi splitting energy between the P + and P-peaks is measured to be $\sim\!200$ meV. To confirm that the high concentration cavity system had entered the strong coupling regime, we used the following equation that defines the magnitude of Rabi splitting required for strong coupling:

$$\hbar\Omega_R > \sqrt{\frac{\Gamma_{UP}^2}{2} + \frac{\Gamma_{LP}^2}{2}} \tag{3}$$

where $\Gamma_{\rm UP}$ and $\Gamma_{\rm LP}$ are the linewidths of the upper and lower polariton branch modes [39]. Fig. 1d shows the baseline-corrected absorption spectra of the high TDBC concentration cavity system taken from Fig. 1c and its spectral separation. The values of $\Gamma_{\rm UB}$ and $\Gamma_{\rm LB}$ are estimated to be 185 meV and 84 meV, corresponding to a $\sqrt{\frac{\Gamma_{\rm UB}^2}{2} + \frac{\Gamma_{\rm LB}^2}{\Gamma_{\rm UB}^2}}$ value of 144 meV. This is smaller than the Rabi splitting energy of ~200 meV, which confirms that the high concentration TDBC cavity has entered the strong coupling regime.

We compared the absorption spectra of the cavity systems to those of the mirror and stand-alone TDBC-PVA control systems to assess the impact of strong coupling on the light absorption (Fig. 1b and c). For the non-cavity samples, where light interacts directly with the TDBC-PVA films, we observe the absorption due to the TDBC electronic transition

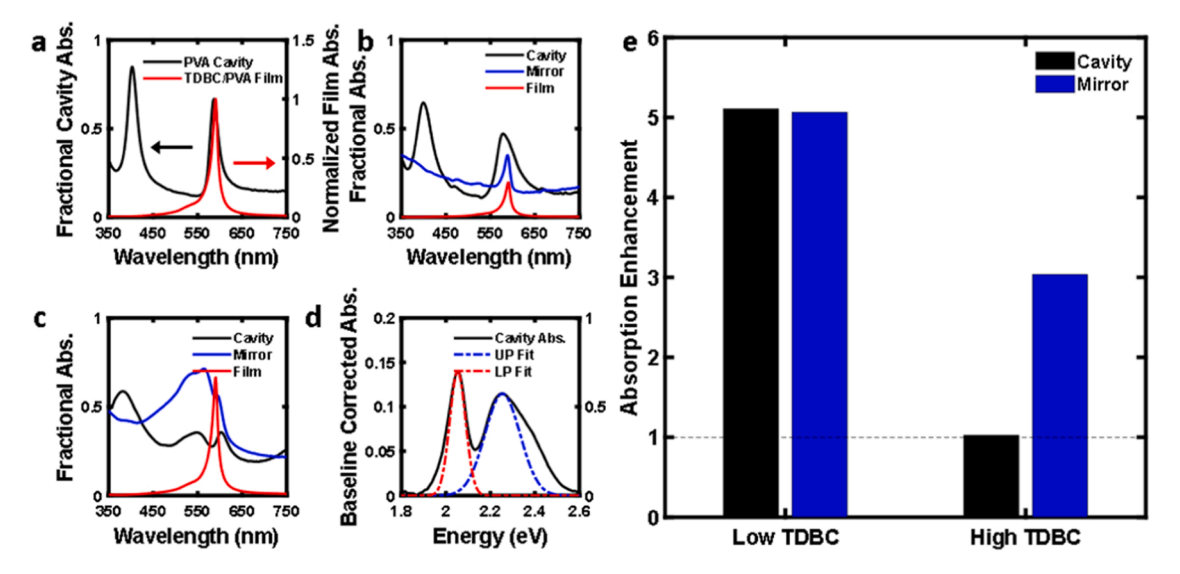


Fig. 1. a) Wavelength-dependent fractional absorption spectra of a PVA cavity tuned to the TDBC resonance at 590 nm (black) and the normalized absorption spectra of a TDBC-PVA film on glass (red). b-c) Experimentally measured fractional absorption spectra for the low concentration (b) and high concentration (c) TDBC-PVA cavity, mirror, and stand-alone film systems. d) The baseline-corrected absorption of the high concentration cavity system and its spectral separation. e) Experimental absorption enhancements calculated for the cavity and mirror systems via Eq. (4).

at 590 nm. In the case of the high concentration TDBC film in the mirror configuration, we observe a broadening of the absorption resulting from reflection off the bottom Ag mirror. To quantify how effective the cavity and mirror systems are at absorbing incident light energy, we calculated an "absorption enhancement" factor where we compare the absorption of these systems to the absorption by the stand-alone TDBC-PVA system via the following equation:

$$AbsEnhancement = \frac{A_{total}}{v_{total}} \times \frac{v_{TDBC}}{A_{TDBC}}$$
 (4)

where Atotal is the total energy absorbed in either the cavity or mirror system, v_{total} is the volume of absorbing material in that system (i.e., Ag layers + TDBC-PVA layer), A_{TDBC} is the total energy absorbed in the stand-alone TDBC-PVA layer (of the same thickness and concentration as the TDBC-PVA layer used in the corresponding cavity or mirror systems), and v_{TDC} is the total volume of just the TDBC-PVA layer in each respective system. We calculated the values of A_{total} and A_{TDBC} by integrating the fractional absorption curves in Fig. 1b-c with respect to energy across the wavelength range of 450 nm to 750 nm, where strong coupling is relevant. The data in Fig. 1e show the volume-normalized absorption enhancement for the cavity and mirror systems compared to their stand-alone TDBC-PVA counterparts. We observe that for the concentration systems, the volume-normalized absorption enhancement is always larger than 1, meaning both the mirror and cavity systems absorb more than the stand-alone TDBC-PVA films at this concentration. In contrast, the data for the high concentration systems show that the absorption enhancement is only greater than one for the mirror configuration.

While the experimental data presented in Fig. 1 shows how effectively these different systems absorb light, they do not give us any information about the system's *local* light absorption rate (i.e., charge carrier generation) in various components (Ag and TDBC). It is usually preferred to absorb light in the desired part of the system (for example, the dye molecules) rather than in the metallic Ag mirrors, where the absorbed energy is dissipated as a parasitic heat loss [42,44]. To answer questions related to the local rates of charge carrier formation, we developed a finite element method (FEM) model and performed simulations on the systems of interest (see supplemental section S2). Our objective was to determine how the rate of charge carrier generation is

distributed throughout the different components of the systems. The FEM model geometry consisted of TDBC-PVA films (of thicknesses corresponding to the experimentally measured thicknesses) sandwiched between a 30 nm Ag top film and 200 nm Ag bottom film for the cavity systems, or without the respective top/bottom Ag films for the mirror and stand-alone TDBC-PVA systems. We measured the dielectric properties for the TDBC-PVA films of varying concentrations using variable angle spectroscopic ellipsometry (see section S3 and Fig. S2) and obtained the dielectric data for Ag from standard databases [45]. We validated the model's accuracy by calculating wavelength-dependent fractional absorption of the high and low concentration cavity/control systems. The calculated spectra in Fig. S3 show good agreement with the experimental spectra presented in Fig. 1. We further confirmed strong light-matter coupling in the high concentration cavity by showing that the upper and lower polariton branches exhibit an anti-crossing as a function of the incident photon angle (Fig. S4).

We used the model to calculate the absorption enhancement factors for the simulated systems using Eq. (4) above. We calculated the total absorption in various components of the system (e.g., the Ag mirrors and the dye layer) by integrating the resistive heating losses within the entire volume of each component across the wavelength range of 450–750 nm. The data in Fig. 2a show good qualitative agreement with the experimental data in Fig. 1e. Differences in the magnitude and relative values are likely a result of experimental error such as inhomogeneities/ roughness in the spin-coated films that are not present in the simulations. We next used the FEM model to shed light on the rate of energy dissipation (i.e., charge carrier excitation) through the TDBC molecules in each system (Fig. 2b-d). We calculated the TDBC absorption enhancement by dividing the total energy absorbed directly in the TDBC layers in each system by the total energy absorbed in a stand-alone TDBC-PVA layer of the same thickness and concentration across the wavelength range of 450-750 nm. The data in Fig. 2b show that the TDBC absorption enhancement for the cavity system is higher than for the mirror system in the case of low concentration. We attribute this enhancement to electric field induced energy transfer from the cavity mode to the TDBC molecules [36,46]. The data also show that the high concentration cavity system (i.e., the strongly coupled system) has lower TDBC absorption enhancements than the mirror systems. The high concentration mirror system exhibits the most prominent enhancement.

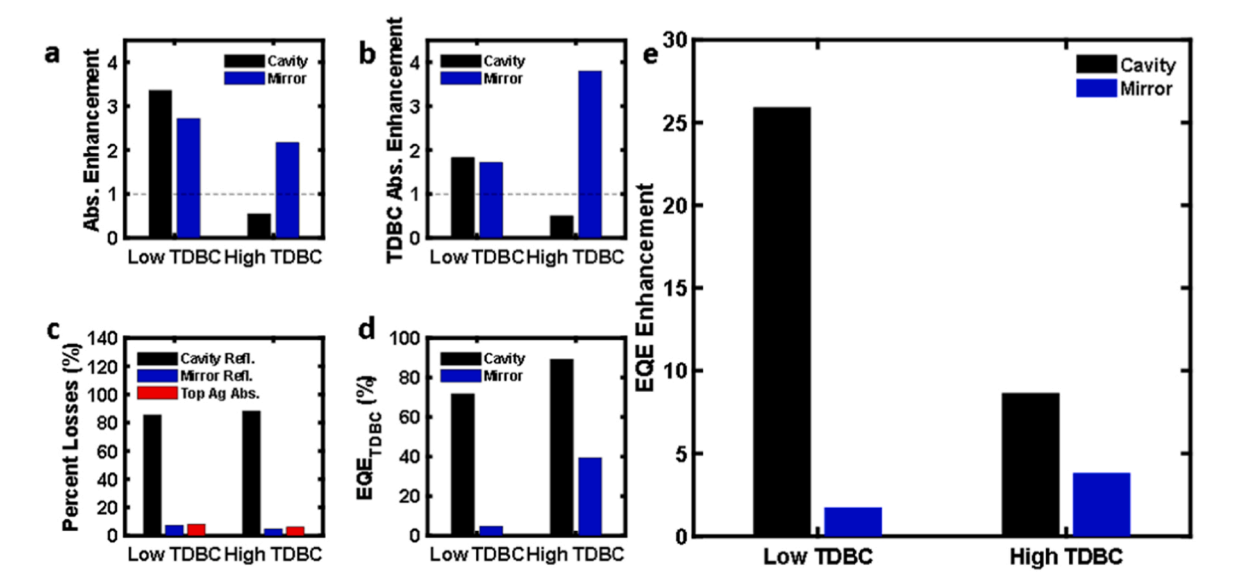


Fig. 2. a) Absorption enhancement calculated for the simulated cavity and mirror systems via Eq. (4). b) The TDBC absorption enhancement calculated for the simulated cavity and mirror systems compared stand-alone TDBC-PVA films of the same thickness and concentration. c) Percentage of energy lost due to reflection (black/red) or absorption within the top Ag mirror (blue) in the simulated cavity and mirror systems. d) Calculated external quantum efficiency for TDBC absorption (EQE_{TDBC}) of the simulated cavity and mirror systems. e) Calculated EQE_{TDBC} enhancement for the simulated cavity and mirror systems.

One crucial aspect to consider when comparing the absorption enhancement of the cavity systems to the mirror systems is related to the presence of the top Ag mirror in the cavity systems. Specifically, losses related to reflection from the top Ag mirror and absorption within the top Ag mirror itself play a significant role in the overall absorption efficiencies of the cavity systems. We quantified these losses by using the FEM model to calculate the fraction of light reflected off the cavity/mirror systems and the absorption losses directly in the top Ag mirror for the cavity systems. The data in Fig. 2c show that introducing a top Ag mirror to form the cavities increases the total reflection losses compared to the mirror systems. These losses increase from ~5% and ~8% (for no top mirror configurations) to ~85% and ~88% (with the top Ag mirror) for the low and high TDBC concentration systems. The 30 nm top Ag mirror results in an additional loss of about 6–8% of the incoming light energy due to parasitic absorption directly in the Ag film.

Next, we investigated how strong coupling affects the local rates of charge carrier excitation in TDBC without these additional losses due to the top Ag mirror. We accomplished this by calculating the absorption external quantum efficiency within the TDBC molecules (EQE_{TDBC}) in the cavity and mirror systems. Specifically, we subtracted the amount of light reflected by and absorbed within the top Ag mirror from the total light impinging on the system to obtain the amount of light directly reaching the TDBC layer for the wavelength range of 450-750 nm. The EQE_{TDBC} was then determined by dividing the amount of light absorbed by the TDBC-PVA layer by the amount of light reaching the TDBC-PVA layer (multiplied by 100). The data in Fig. 2d show that the cavity system surpasses the mirror system efficiencies for both the low and high TDBC concentrations, with the strongly coupled cavity reaching an EQE_{TDBC} value of ~89%. While this data suggests that entering the strong coupling regime enhances the light absorption EQE within these molecular dyes, we need to consider that simply increasing the concentration of molecules in the cavity increases the absorption in the system. To normalize for this concentration effect, we calculated the enhancement in EQE for the cavity and mirror systems by dividing their EQE by the EQE for the stand-alone TDBC film of equivalent concentration. The data in Fig. 2e show that the cavity systems exhibit much higher EQE than the mirror systems, with the lowest concentration systems exhibiting the largest enhancement.

Our analysis presented in Fig. 2 allows us to postulate the optimal system for directing light energy into molecules or other absorbers. We hypothesized that an open system with strongly coupled absorbers directly interacting with the incoming photon flux would yield the highest light absorption efficiencies. The corollary to this hypothesis is that these open systems would be ideal for enhancing light absorption in extremely thin films of molecular absorbers (i.e., tens of nanometers and less), which we expect to absorb poorly even in the mirror configuration. This corollary stems from the data in Fig. 2, where the low concentration systems (which are inherently poor absorbers) exhibit the most significant EQE enhancements. As we noted above, enhancing the absorption rates in exceptionally thin layers of material is critical for various applications, including photovoltaics and photocatalysis [38,47–49].

We tested these hypotheses by using the FEM model to study the light absorption rates within TDBC-PVA films of decreasing thickness deposited on an Ag film containing a hexagonal array of nanoholes. The Ag nanohole array system couples incoming light to the metal film via a grating coupling mechanism. This coupling results in surface plasmon polaritons (SPP) that significantly enhance the electromagnetic field confinement to the surface of the Ag array. Coupling molecules to these SPP modes can give rise to strong light-matter coupling similar to the coupling of Fabry-Perot cavities [50–52]. We tune the SPP wavelength (λ_{sp}) of the nanohole array for a constant Ag film thickness and nanohole diameter (D) by varying the periodicity (P) of the nanoholes. We note that the optical signature of the plasmon resonance for these array systems is a peak in the nanohole transmission (and absorption) spectra [53,54].

We chose the model parameters to ensure the TDBC-PVA thin films

coupled to the Ag nanohole array system entered the strong coupling regime. We set the Ag film thickness for the array systems to 200 nm and varied the thickness of the TDBC-PVA layer on top of the array from 40 nm to 5 nm. We set D to 130 nm, and P was varied to ensure λ_{sp} overlapped with the TDBC electronic transition at 590 nm (Table S1). Finally, we set the dielectric properties for the TDBC-PVA films equal to those experimentally extracted from a 66 wt% TDBC-PVA film (Fig. S5). These parameters were used in the FEM model to study the effectiveness of these systems to localize the absorption process into these molecular dyes.

The data in Fig. 3a show the simulated absorption spectra for the TDBC-PVA nanohole array systems with varying film thicknesses. We observe a peak centered at 590 nm for all systems due to absorption from uncoupled TDBC molecules. We also observe the emergence of strongly coupled P + and P- peaks for each system, where the Rabi splitting increases with increasing film thickness due to the higher number of coupled TDBC molecules. To ensure these systems have entered the strong coupling regime, we compared the Rabi splitting energy of the thinnest TDBC-PVA array system (~181.5 meV) with the linewidths of its upper and lower polariton branches via Eq. (3). The data in Fig. S6 show that the linewidths of the P + and P- branches correspond to $\Gamma_{\rm UP}$ and $\Gamma_{\rm LP}$ values of 76.89 meV and 60.91 meV, respectively, which results in a $\sqrt{\frac{\Gamma_{\rm LP}^2}{2} + \frac{\Gamma_{\rm LP}^2}{2}}$ value of 69.7 meV. This analysis confirms that these systems have entered the strong coupling regime.

We next calculated EQE_{TDBC} for these systems as described above (we note that there is no top Ag mirror in these systems). We plotted the calculated EQE_{TDBC} in Fig. 3b along with the EQE_{TDBC} for the corresponding control systems. The data show that the nanohole array systems coupled to TDBC exhibit significantly higher EQE_{TDBC} values than their corresponding mirror and stand-alone TDBC-PVA systems. The EQE_{TDBC} is highest for the thickest TDBC-PVA film (40 nm), which approaches 37%, compared to 19% for the mirror system and 13% for the respective stand-alone TDBC-PVA layer. This analysis supports our hypotheses that strongly coupled open systems enhance molecular absorption compared to their mirror counterparts.

Additionally, we calculated the EQE_{TDBC} enhancement for the array and mirror configurations of varying TDBC-PVA layer thickness relative to the stand-alone TDBC system and plotted them in Fig. 3c. We observe that the highest enhancements in TDBC absorption compared to the stand-alone TDBC-PVA films occur for the thinnest samples. These observations demonstrate that entering the strong coupling regime is critical for designing systems that localize energetic charge carrier formation rates in increasingly small volumes. We can see this in Fig. 3d, where we plot the TDBC-PVA layer thicknesses required for the mirror and stand-alone film configurations to reach the same EQE_{TDBC} as the array configuration with identical TDBC-PVA layer thickness and concentration. The data show that for the 40 nm TDBC-PVA thickness, the film thicknesses required to reach the same EQE_{TDBC} as the array system are \sim 75 nm and \sim 107 nm for the mirror and stand-along systems, respectively.

We also studied the impact of the TDBC concentration on the absorption rates within a TDBC-PVA film of a constant thickness (40 nm) coupled to a nanohole array. The TDBC-PVA optical properties were obtained by preparing spin-coated films from solutions of varying TDBC concentration (20 wt% TDBC, 33 wt% TDBC, 50 wt% TDBC, and 66 wt % TDBC) and extracting their optical properties via ellipsometry. We set the array geometric parameters equal to those presented above, except we adjusted P to ensure the array systems were resonant with the TDBC electronic transition for each concentration film.

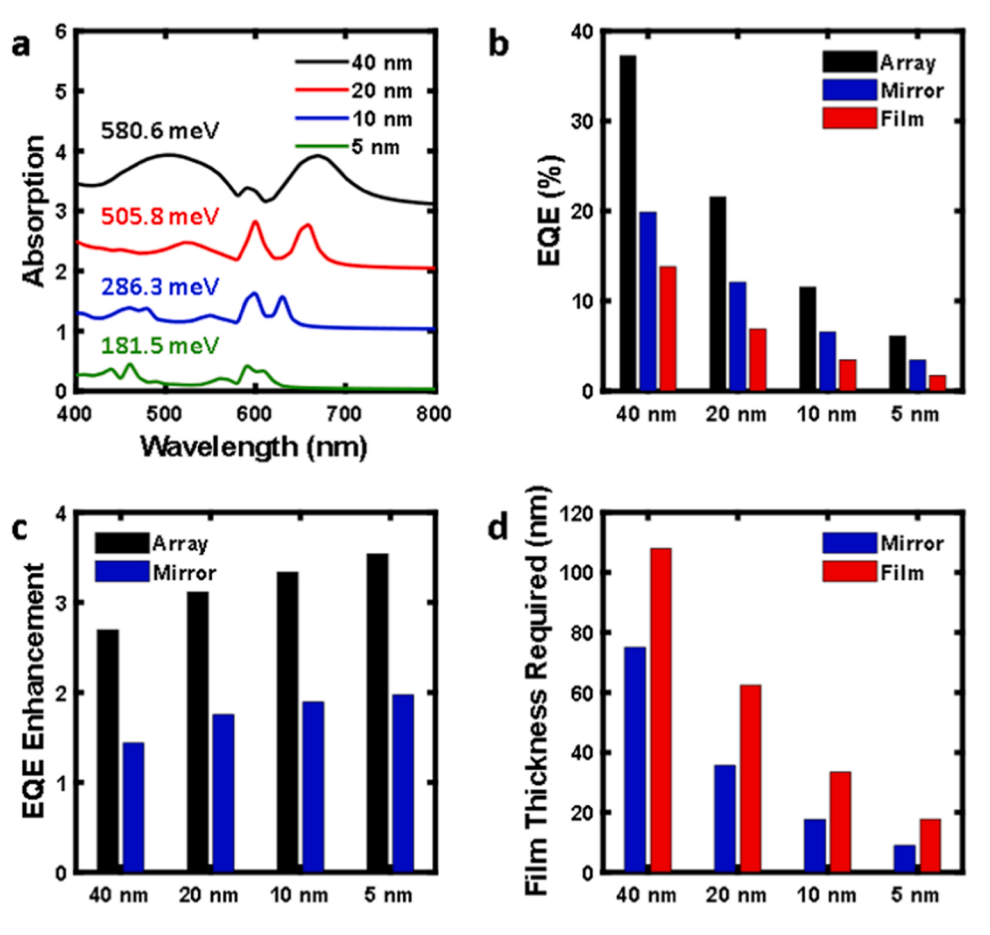


Fig. 3. a) Simulated fractional absorption spectra of TDBC-PVA films of varying thicknesses coupled to a Ag nanohole array. We show the values of the absorption Rabi splitting next to each spectrum. We vertically offset the spectra for improved visibility. b) Calculated EQE_{TDBC}'s of the simulated TDBC-PVA nanohole array systems of varying thicknesses compared to the corresponding mirror systems and stand-alone TDBC-PVA systems of the same thickness and concentration. c) Calculated EQE_{TDBC} enhancement for the simulated nanohole array and mirror systems of varying thickness. d) Film thicknesses required to achieve the same EQE_{TDBC} as a TDBC-PVA layer at a given thickness strongly coupled to the Ag nanohole array for both the mirror and standalone film configurations.

verify this by plotting the absorption Rabi splitting as a function of the square root of the TDBC concentration in the TDBC-PVA films. The data in Fig. 4b show that the Rabi splitting exhibits a linear dependence on the square root of the TDBC concentration, following Eq. (2) above. This analysis confirms that these systems have entered the strong coupling regime.

We used the model to study energy dissipation rates through the 40 nm TDBC-PVA films of varying concentrations coupled to the nanohole array. We compared these rates to the energy dissipation rates through TDBC-PVA films in the mirror and stand-alone TDBC-PVA film configurations of the same thickness and TDBC concentration. We calculated the total power dissipated within the TDBC-PVA layer for these array, mirror, and stand-alone systems by summing the power absorbed throughout the TDBC layer at each wavelength from 450–750 nm and plotted it as a function of TDBC concentration (Fig. 4c). The data show that the power dissipated through TDBC in the array systems is significantly higher than in the mirror and stand-alone TDBC-PVA systems. In these control systems, the power dissipation (absorption) in the TDBC layer exhibits a linear dependence on the TDBC concentration, as expected from Beer's law.

Interestingly, the power dissipation throughout TDBC layers coupled to the nanohole arrays is nonlinear with respect to the TDBC concentration. Upon coupling the TDBC film to the nanohole array, we observe a significant initial increase at low concentrations that beings to plateau at higher concentrations. The data in Fig. S7 show that the power dissipated through the TDBC-PVA films coupled to the array systems exhibits a linear dependence on the square root of the TDBC concentration. This concentration dependence is unique to the strongly coupled films and demonstrates how strong coupling can modify the absorption characteristics in molecular films compared to the weak coupling regime. Additionally, we plotted the enhancement in the total power

dissipation throughout the TDBC-PVA films in the array configuration at a given concentration compared to the mirror and stand-alone TDBC-PVA configurations at the equivalent concentration. The data in Fig. 4d again show that the enhancements are most prominent for the low concentration systems.

3. Conclusion

The analysis above paints a comprehensive picture of light absorption within molecular thin films coupled to photonic nanostructures. By analyzing the light absorption rates within thin films of dye molecules strongly coupled to Fabry-Perot optical cavities, we demonstrate that light absorption within the molecular layer is highest in systems free from extraneous absorbers that could lead to parasitic absorption losses. We corroborate this by studying the light absorption rates of molecular thin films coupled to plasmonic nanohole arrays. By varying the molecular concentration within the films, we show that molecules strongly coupled to the arrays exhibit the most significant rates of molecular light absorption compared to weakly coupled systems. We additionally show that strong coupling is ideal for enhancing light absorption in optically thin films by varying the thickness of the films coupled to the arrays. We note that the efficiency enhancement relative to other systems becomes limited at high concentrations (or large thicknesses) due to the ability of the uncoupled systems to absorb increasing amounts of light energy under these conditions. This limited absorption enhancement at high concentrations is also inherently limited by the square root dependence of the power dissipation within TDBC on the molecular concentration, which we show is unique to the strong coupling regime. Overall, these findings provide guidelines for exploiting strong light-matter coupling to improve both traditional solar energy conversion technologies that rely on localizing the charge carrier generation process into small volumes of

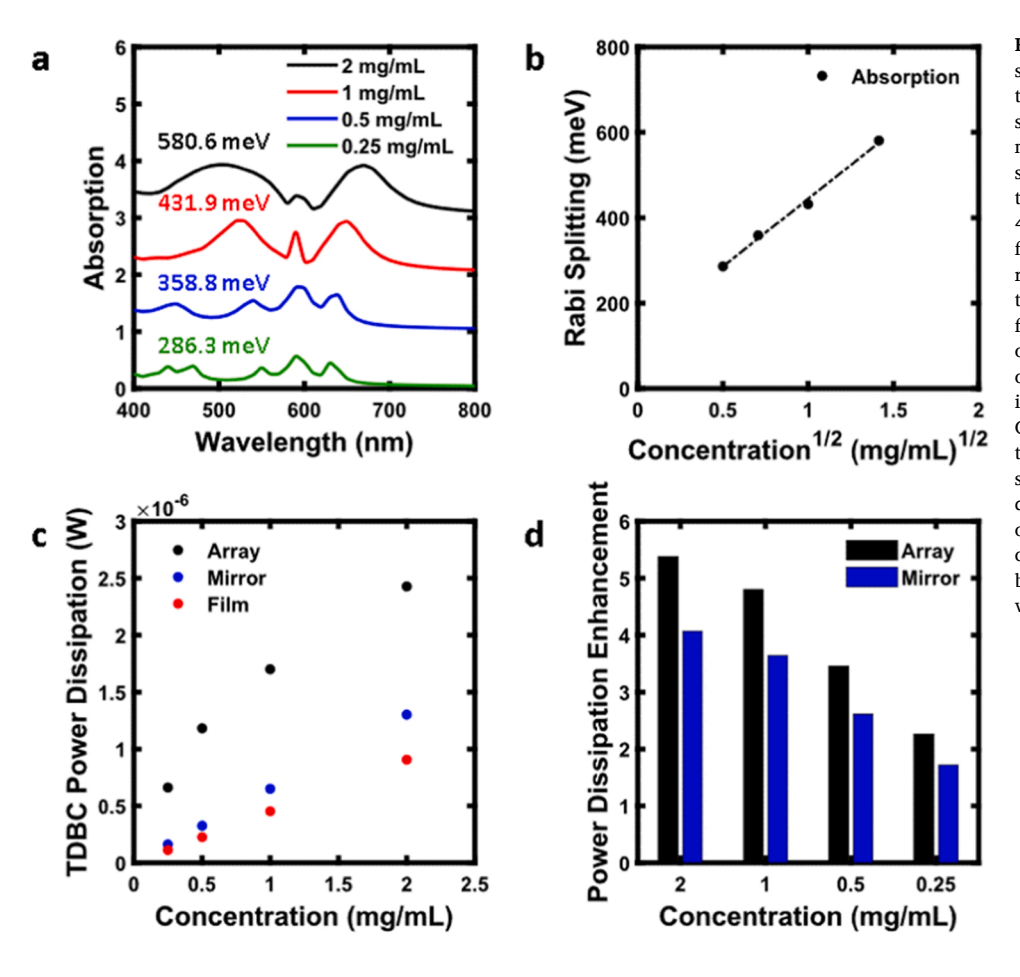


Fig. 4. a) Simulated fractional absorption spectra of TDBC-PVA films of varying concentrations coupled with a Ag nanohole array. We show the values of the absorption Rabi splitting next to each spectrum. We vertically offset the spectra for improved visibility. b) The value of the absorption Rabi splitting for the simulated 40 nm TDBC-PVA nanohole array systems as a function of the TDBC film concentration square root. c) The total power dissipated throughout the TDBC-PVA films as a function of the TDBC film concentration in either the array, mirror, or film configuration for the wavelength range of 450-750 nm. At each wavelength, the power input into the model was 2.1×10^{-7} W. d) Calculated power dissipation enhancement for the simulated 40 nm TDBC-PVA nanohole array systems of varying TDBC concentration. In (ad), the concentration of TDBC is listed in units of mg TDBC/mL water used to prepare the spin coating solution. The amount of PVA used can be calculated from the corresponding wt% values listed in the text.

material and novel polariton-based solar energy conversion systems that rely on the unique properties of photoexcited polaritons to operate at unprecedented efficiencies [55,56].

CRediT authorship contribution statement

S.C. and S.L. developed the project. S.C. performed the optical characterization/measurements and performed the finite element modeling. All authors wrote the manuscript and the supplementary information.

Declaration of Competing Interest

The authors declare that they have no known competing financial interests or personal relationships that could have appeared to influence the work reported in this paper.

Acknowledgments

This research was supported by the U.S. Department of Energy, Office of Science, Office of Basic Energy Sciences, under Award (DE-SC0021362) (experimental work) and National Science Foundation (NSF) (CBET-1803991) (modeling work). Secondary support for the development of analytical tools used in the model was provided by NSF (CBET-1702471 and CHE-1800197).

Supporting Information

The supporting information presents the schematic of the model systems, details of the finite element simulations, dielectric information used in the models, and confirmation of nanohole array coupling.

Appendix A. Supporting information

Supplementary data associated with this article can be found in the online version at doi:10.1016/j.nanoen.2022.107244.

References

- M.S. Skolnick, T.A. Fisher, D.M. Whittaker, Strong coupling phenomena in quantum microcavity structures, Semicond. Sci. Technol. 13 (1998) 645–669, https://doi.org/10.1088/0268-1242/13/7/003.
- [2] J. Kasprzak, M. Richard, S. Kundermann, A. Baas, P. Jeambrun, J.M.J. Keeling, F. M. Marchetti, M.H. Szymańska, R. André, J.L. Staehli, V. Savona, P.B. Littlewood, B. Deveaud, L.S. Dang, Bose–Einstein condensation of exciton polaritons, Nature 443 (2006) 409–414, https://doi.org/10.1038/nature05131.
- [3] J.M. Raimond, M. Brune, S. Haroche, Colloquium: manipulating quantum entanglement with atoms and photons in a cavity, Rev. Mod. Phys. 73 (2001) 565–582, https://doi.org/10.1103/RevModPhys.73.565.
- [4] P. Törmä, W.L. Barnes, Strong coupling between surface plasmon polaritons and emitters: a review, Rep. Prog. Phys. 78 (2015), 013901, https://doi.org/10.1088/ 0034-4885/78/1/013901.
- [5] P. Vasa, C. Lienau, Strong light-matter interaction in quantum emitter/metal hybrid nanostructures, ACS Photonics 5 (2018) 2–23, https://doi.org/10.1021/ acsphotonics.7b00650.
- [6] T.W. Ebbesen, Hybrid light-matter states in a molecular and material science perspective, Acc. Chem. Res. 49 (2016) 2403–2412, https://doi.org/10.1021/acs. accounts 6b00295
- [7] B. Kolaric, B. Maes, K. Clays, T. Durt, Y. Caudano, Strong light–matter coupling as a new tool for molecular and material engineering: quantum approach, Adv. Quantum Technol. 1 (2018), 1800001, https://doi.org/10.1002/ OUTF.201800001.
- [8] D.G. Baranov, M. Wersa, J. Cuadra, T.J. Antosiewicz, T. Shegai, Novel nanostructures and materials for strong light—matter interactions, ACS Photonics (2018) 24–42. https://doi.org/10.1021/acsphotonics.7b00674.
- [9] M. Hertzog, M. Wang, J. Rgen Mony, K. Bö, Strong light-matter interactions: a new direction within chemistry, Chem. Soc. Rev. 48 (2019) 937–961, https://doi.org/ 10.1039/c8cs00193f.
- [10] E.M. Purcell, Spontaneous emission probabilities at radio frequencies, Phys. Rev. 69 (1946). (http://pages.erau.edu/~reynodb2/colloquia/Purcell_1946_Spontan eousEmission.pdf). accessed January 22, 2020.

- [11] D.S. Dovzhenko, S.V. Ryabchuk, Y.P. Rakovich, I.R. Nabiev, Light-matter interaction in the strong coupling regime: configurations, conditions, and applications, Nanoscale 10 (2018), https://doi.org/10.1039/c7nr06917k.
- [12] D. Sanvitto, S. Kéna-Cohen, The road towards polaritonic devices, Nat. Mater. 15 (2016) 1061–1073, https://doi.org/10.1038/nmat4668.
- [13] J.A. Hutchison, A. Liscio, T. Schwartz, A. Canaguier-Durand, C. Genet, V. Palermo, P. Samori, T.W. Ebbesen, Tuning the work-function via strong coupling, Adv. Mater. 25 (2013) 2481–2485, https://doi.org/10.1002/adma.201203682.
- [14] D.M. Coles, N. Somaschi, P. Michetti, C. Clark, P.G. Lagoudakis, P.G. Savvidis, D. G. Lidzey, Polariton-mediated energy transfer between organic dyes in a strongly coupled optical microcavity, Nat. Mater. 13 (2014) 712–719, https://doi.org/10.1038/NMAT3950
- [15] X. Zhong, T. Chervy, L. Zhang, A. Thomas, J. George, C. Genet, J.A. Hutchison, T. W. Ebbesen, Energy transfer between spatially separated entangled molecules, Angew. Chem. Int. Ed. Engl. 56 (2017) 9034–9038, https://doi.org/10.1002/anje.201703539
- [16] X. Zhong, T. Chervy, S. Wang, J. George, A. Thomas, J.A. Hutchison, E. Devaux, C. Genet, T.W. Ebbesen, Non-radiative energy transfer mediated by hybrid lightmatter states, Angew. Chem. Int. Ed. 55 (2016) 6202–6206, https://doi.org/ 10.1002/anie.201600428.
- [17] G.G. Rozenman, K. Akulov, A. Golombek, T. Schwartz, Long-range transport of organic exciton-polaritons revealed by ultrafast microscopy, ACS Photonics 5 (2018) 105–110, https://doi.org/10.1021/acsphotonics.7b01332.
- [18] K. Georgiou, P. Michetti, L. Gai, M. Cavazzini, Z. Shen, D.G. Lidzey, Control over energy transfer between fluorescent bodipy dyes in a strongly coupled microcavity, ACS Photonics 5 (2018) 258–266, https://doi.org/10.1021/acsphotonics.7b01002.
- [19] P. Zeng, J. Cadusch, D. Chakraborty, T.A. Smith, A. Roberts, J.E. Sader, T.J. Davis, D.E. Gómez, Photoinduced electron transfer in the strong coupling regime: waveguide–plasmon polaritons, Nano Lett. 16 (2016) 2651–2656, https://doi.org/ 10.1021/acs.nanolett.6b00310.
- [20] H. Shan, Y. Yu, X. Wang, Y. Luo, S. Zu, B. Du, T. Han, B. Li, Y. Li, J. Wu, F. Lin, K. Shi, B.K. Tay, Z. Liu, X. Zhu, Z. Fang, Direct observation of ultrafast plasmonic hot electron transfer in the strong coupling regime, Light Sci. Appl. 8 (2019) 9, https://doi.org/10.1038/s41377-019-0121-6.
- [21] E. Orgiu, J. George, J.A. Hutchison, E. Devaux, J.F. Dayen, B. Doudin, F. Stellacci, C. Genet, J. Schachenmayer, C. Genes, G. Pupillo, P. Samori, T.W. Ebbesen, Conductivity in organic semiconductors hybridized with the vacuum field, Nat. Mater. 14 (2015) 1123–1130, https://doi.org/10.1038/NMAT4392.
- [22] K. Nagarajan, J. George, A. Thomas, E. Devaux, T. Chervy, S. Azzini, J. Aziz, M. W. Hosseini, A. Kumar, C. Genet, N. Bartolo, C. Ciuti, T. Ebbesen, Conductivity and photoconductivity of a p-type organic semiconductor under ultra-strong coupling, ACS Nano 14 (2020) 10219–10225, https://doi.org/10.26434/chemrxiv.7498622.
- [23] D. Hagenmüller, J. Schachenmayer, S. Schütz, C. Genes, G. Pupillo, Cavity-enhanced transport of charge, Phys. Rev. Lett. 119 (2017), 223601, https://doi.org/10.1103/PhysRevLett.119.223601.
- [24] A. Canaguier-Durand, E. Devaux, J. George, Y. Pang, J.A. Hutchison, T. Schwartz, C. Genet, N. Wilhelms, J.-M. Lehn, T.W. Ebbesen, Thermodynamics of molecules strongly coupled to the vacuum field, Angew. Chem. Int. Ed. 52 (2013) 10533–10536, https://doi.org/10.1002/anie.201301861.
- [25] T. Schwartz, J.A. Hutchison, C. Genet, T.W. Ebbesen, Reversible switching of ultrastrong light-molecule coupling, Phys. Rev. Lett. 106 (2011), 196405, https:// doi.org/10.1103/PhysRevLett.106.196405.
- [26] J.A. Hutchison, T. Schwartz, C. Genet, E. Devaux, T.W. Ebbesen, Modifying chemical landscapes by coupling to vacuum fields, Angew. Chem. Int. Ed. 51 (2012) 1592–1596, https://doi.org/10.1002/anie.201107033.
- [27] B. Munkhbat, M. Wersäll, D.G. Baranov, T.J. Antosiewicz, T. Shegai, Suppression of photo-oxidation of organic chromophores by strong coupling to plasmonic nanoantennas, Sci. Adv. 4 (2018) eaas9552. (http://advances.sciencemag.org/). accessed January 7, 2019.
- [28] A. Thomas, L. Lethuillier-Karl, K. Nagarajan, R.M.A. Vergauwe, J. George,
 T. Chervy, A. Shalabney, E. Devaux, C. Genet, J. Moran, T.W. Ebbesen, Tilting a
 ground-state reactivity landscape by vibrational strong coupling, Science 80 (363) (2019) 615–619, https://doi.org/10.1126/SCIENCE.AAU7742.

 [29] K. Hirai, J.A. Hutchison, H. Uji-i, Recent progress in vibropolaritonic chemistry,
- [29] K. Hirai, J.A. Hutchison, H. Uji-i, Recent progress in vibropolaritonic chemistry, Chempluschem 85 (2020) 1981–1988, https://doi.org/10.1002/cplu.202000411
- [30] H. Hiura, A. Shalabney, J. George, H. Hiura, A. Shalabney, J. George, Cavity Catalysis — Accelerating Reactions under Vibrational Strong Coupling —, (2018). https://doi.org/10.26434/chemrxiv.7234721.v2.
- [31] J.A. Schuller, E.S. Barnard, W. Cai, Y.C. Jun, J.S. White, M.L. Brongersma, Plasmonics for extreme light concentration and manipulation, Nat. Mater. 9 (2010) 193–204, https://doi.org/10.1038/nmat2630.
- [32] M. Moskovits, The case for plasmon-derived hot carrier devices, Nat. Nanotechnol. 10 (2015) 6–8, https://doi.org/10.1038/nnano.2014.280.
- [33] J.C. Ndukaife, V.M. Shalaev, A. Boltasseva, Plasmonics-turning loss into gain, Science 80-. (351) (2016) 334–335, https://doi.org/10.1126/science.aad9864
- [34] C. Clavero, Plasmon-induced hot-electron generation at nanoparticle/metal-oxide interfaces for photovoltaic and photocatalytic devices, Nat. Photonics 8 (2014) 95–103, https://doi.org/10.1038/nphoton.2013.238.
- [35] U. Aslam, V.G. Rao, S. Chavez, S. Linic, Catalytic conversion of solar to chemical energy on plasmonic metal nanostructures, Nat. Catal. 1 (2018) 656–665, https:// doi.org/10.1038/s41929-018-0138-x.
- [36] S. Linic, S. Chavez, R. Elias, Flow and extraction of energy and charge carriers in hybrid plasmonic nanostructures, Nat. Mater. 20 (2021) 916–924, https://doi.org/ 10.1038/s41563-020-00858-4.

- [37] M.L. Brongersma, N.J. Halas, P. Nordlander, Plasmon-induced hot carrier science and technology, Nat. Nanotechnol. 10 (2015) 25–34, https://doi.org/10.1038/ nnano.2014.311.
- [38] U. Aslam, S. Chavez, S. Linic, Controlling energy flow in multimetallic nanostructures for plasmonic catalysis, Nat. Nanotechnol. 12 (2017) 1000–1005, https://doi.org/10.1038/NNANO.2017.131.
- [39] X. Shi, K. Ueno, T. Oshikiri, Q. Sun, K. Sasaki, H. Misawa, Enhanced water splitting under modal strong coupling conditions, Nat. Nanotechnol. (2018) 1, https://doi. org/10.1038/s41565-018-0208-x.
- [40] D.E. Gómez, X. Shi, T. Oshikiri, A. Roberts, H. Misawa, Near-perfect absorption of light by coherent plasmon–exciton states, Nano Lett. 21 (2021) 3864–3870, https://doi.org/10.1021/acs.nanolett.1c00389.
- [41] Q. Shang, C. Li, S. Zhang, Y. Liang, Z. Liu, X. Liu, Q. Zhang, Enhanced optical absorption and slowed light of reduced-dimensional CsPbBr3 nanowire crystal by exciton-polariton, Nano Lett. 20 (2020) 1023–1032, https://doi.org/10.1021/ACS. NANOLETT.9B04175/SUPPL. FILE/NL9B04175 SI 001.PDF.
- [42] J.B. Khurgin, How to deal with the loss in plasmonics and metamaterials, Nat. Nanotechnol. 10 (2015), https://doi.org/10.1038/nnano.2014.310.
- [43] Q. Li, J. Lu, P. Gupta, M. Qiu, Engineering optical absorption in graphene and other 2D materials: advances and applications, Adv. Opt. Mater. 7 (2019), 1900595, https://doi.org/10.1002/ADOM.201900595.
- [44] S.A. Maier, Plasmonics: Fundamentals and applications, 2007. https://doi.org/1 0.1007/0-387-37825-1.
- [45] A.D. Rakić, A.B. Djurišić, J.M. Elazar, M.L. Majewski, Optical properties of metallic films for vertical-cavity optoelectronic devices, Appl. Opt. 37 (1998) 5271, https://doi.org/10.1364/AO.37.005271
- [46] J. Li, S.K. Cushing, F. Meng, T.R. Senty, A.D. Bristow, N. Wu, Plasmon-induced resonance energy transfer for solar energy conversion, Nat. Photonics 9 (2015) 601–607, https://doi.org/10.1038/nphoton.2015.142.
- [47] H. Atwater, A. Polman, Plasmonics for improved photovoltaic devices, Nat. Mater. 9 (2010) 205–213, https://doi.org/10.1038/nmat2866.
- [48] S. Chavez, U. Aslam, S. Linic, Design principles for directing energy and energetic charge flow in multicomponent plasmonic nanostructures, ACS Energy Lett. 3 (2018) 1590–1596, https://doi.org/10.1021/acsenergylett.8b00841.
- [49] S. Chavez, V.G. Rao, S. Linic, Unearthing the factors governing site specific rates of electronic excitations in multicomponent plasmonic systems and catalysts, Faraday Discuss. 214 (2019) 441–453, https://doi.org/10.1039/C8FD00143J.
- [50] A. Salomon, C. Genet, T.W. Ebbesen, Molecule-light complex: dynamics of hybrid molecule-surface plasmon states, Angew. Chem. Int. Ed. 48 (2009) 8748–8751, https://doi.org/10.1002/anie.200903191.
- [51] A. Salomon, S. Wang, J.A. Hutchison, C. Genet, T.W. Ebbesen, Strong light-molecule coupling on plasmonic arrays of different symmetry, ChemPhysChem 14 (2013) 1882–1886, https://doi.org/10.1002/cphc.201200914.
- [52] E.S. Kang, S. Chen, S. Sardar, D. Tordera, N. Armakavicius, V. Darakchieva, T. Shegai, M.P. Jonsson, Strong plasmon–exciton coupling with directional absorption features in optically thin hybrid nanohole metasurfaces, ACS Photo 5 (2018) 4046–4055, https://doi.org/10.1021/acsphotonics.8b00679.
- [53] T.W. Ebbesen, H.J. Lezec, H.F. Ghaemi, T. Thio, P.A. Wolff, Extraordinary optical transmission through sub-wavelenght hole arrays, Nature 391 (1998) 667–669, https://doi.org/10.1038/35570.
- [54] C. Genet, T.W. Ebbesen, Light in tiny holes, Nature 445 (2007) 39–46, https://doi. org/10.1038/nature05350.
- [55] V.C. Nikolis, A. Mischok, B. Siegmund, J. Kublitski, X. Jia, J. Benduhn, U. Hörmann, D. Neher, M.C. Gather, D. Spoltore, K. Vandewal, Strong light-matter coupling for reduced photon energy losses in organic photovoltaics, 2019 101. Nat. Commun. 10 (2019) 1–8, https://doi.org/10.1038/s41467-019-11717-5.
- [56] C. Bujalance, V. Esteso, L. Caliò, G. Lavarda, T. Torres, J. Feist, F.J. García-Vidal, G. Bottari, H. Míguez, Ultrastrong exciton–photon coupling in broadband solar absorbers, J. Phys. Chem. Lett. 12 (2021) 10706–10712, https://doi.org/10.1021/ ACS_JPCLETT.1C02898.



Steven Chavez received his B.S. in chemical engineering from UC Berkeley and his M.S.and Ph.D. from the University of Michigan under the direction of Professor Suljo Linic as both a NSF Graduate Research Fellow and a Ford Foundation Fellow. He is currently a postdoctoral researcher in the group of Professor Matteo Cargnello at Stanford University. His research interests broadly intersect at the interface between nanophotonics, heterogenous catalysis, andthe exploitation of lightmatter interactions to enable next generation of solar energy conversion technologies.



Suljo Linic received his Ph.D. degree in chemical engineering at the University of Delaware in 2004 after receiving his B.S. degree in Physics with a minor in Mathematics and Chemistry from West Chester University in West Chester (PA). He was a Max Planck postdoctoral fellow at thetheory department at the Fritz Haber Institute of Max Planck Society in Berlin (Germany). He is currently the Martin Lewis Perl Collegiate Professor of Chemical Engineering at the University of Michigan in Ann Arbor. He has alsoheld an appointment as a Hans Fischer Fellow at the chemistry department of the Technical University Munich. His work focuses on light-matter interactions, photoelectrocatalysis, electrocatalysis and thermal catalysis.